Supplementary material

Large-Area Metal-Integrated Grating Electrode Achieving Near 100% Infrared Transmission

Karolina Bogdanowicz,[1,2] Weronika Głowadzka,[1,2] Tristan Smołka,[3] Michał Rygała,[3] Marcin Kałuża,[4] Marek Ekielski,[1] Oskar Sadowski,[1,5] Magdalena Zadura,[1,2] Magdalena Marciniak,[2] Marcin Gębski,[2] Michał Wasiak,[2] Marcin Motyka,[3] Anna Szerling,[1] and Tomasz Czyszanowski[2,*]

[1] *Łukasiewicz Research Network – Institute of Microelectronics and Photonics, al. Lotników 32/46, 02-668 Warsaw, Poland*

[2] *Photonics Group, Institute of Physics, Lodz University of Technology, ul. Wólczańska 219, 90-924 Łódź, Poland*

[3] *Laboratory for Optical Spectroscopy of Nanostructures, Department of Experimental Physics, Faculty of Fundamental Problems of Technology, Wrocław University of Science and Technology, Wybrzeże Wyspiańskiego 27, 50-370 Wrocław, Poland*

[4] *Institute of Electronics, Lodz University of Technology, al. Politechniki 8, 93-590 Łódź, Poland*

[5] *Warsaw University of Technology – Institute of Microelectronics and Optoelectronics, 00-662 Warsaw, Koszykowa 75, Poland*

This PDF file includes:

- Supporting figures S1–S7
- Supporting information S1, S2, S3

* tomasz.czyszanowski@p.lodz.pl

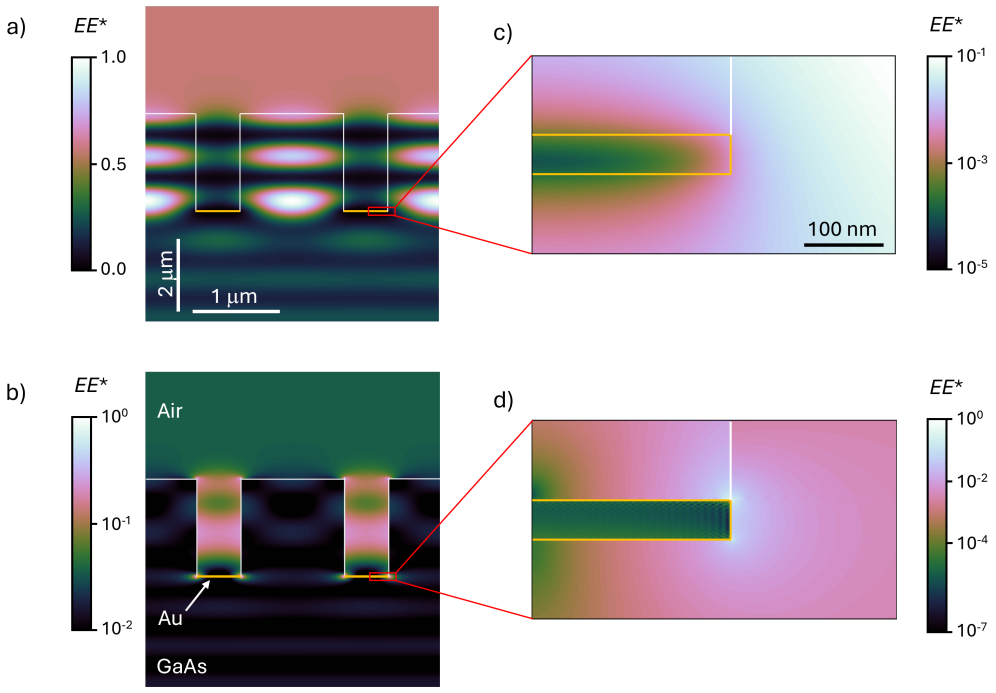

Figure S1. Light intensity (EE^*) distribution under normal incidence from the substrate side in the case of a), c) TE and b), d) TM polarization in the yz-plane of the metalMHCG cross-section, c) and d) are zoomed distributions in the proximity of metal.

S1. MEASUREMENT SETUP

Transmittance measurements were conducted using a Vertex 80v vacuum Fourier Transform Infrared spectrometer (FTIR) from Bruker. Due to the many limitations and difficulties of working in the mid-infrared spectral region, it was necessary to use a Fourier spectrometer instead of a simpler monochromator-based setup. The advantages of using the FTIR approach over the dispersive setup have been extensively studied and described [1–4]. Figure S4a shows the experimental setup for transmittance measurements. The sample light generated by a polychromatic source (either a halogen or a glow bar, depending on the spectral range) was guided by parabolic golden mirrors to the Michelson interferometer and then focused onto the sample at a normal incident angle, creating a roughly 1-mm diameter spot entirely contained within the metalMHCG sample. The sample was placed on a mounting holder with a slit slightly larger than the diameter of the focused spot, which allowed light to transmit through the entire sample and exit from the etched grating. The transmitted

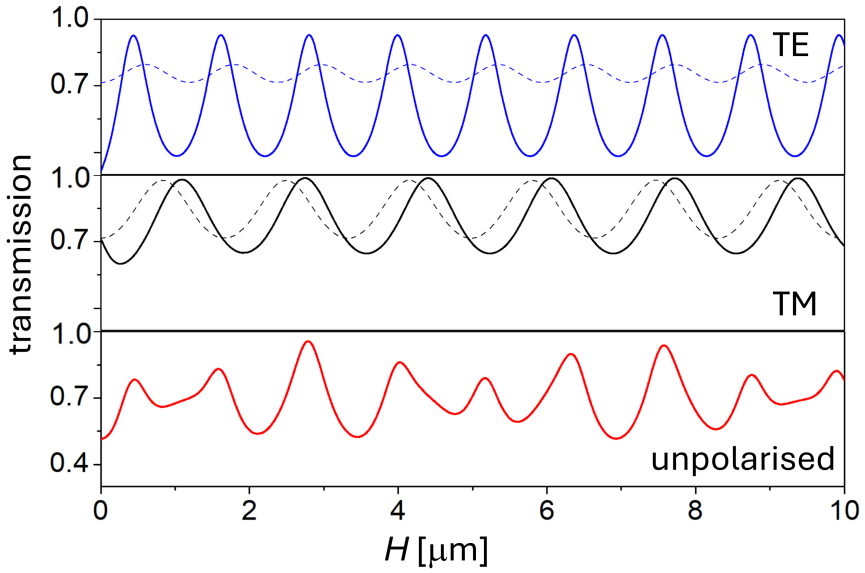

Figure S2. Calculated transmission of both polarisations (solid lines blue and black) and unpolarized light (solid line red) as a function of semiconductor stripe height in the metalMHCG for L =1.4 µm, $F = 0.74$, $H_{\mathrm{m}} = 50$ nm and a wavelength of 7 µm. Dashed lines represent transmission through semi-infinite GaAs with a homogeneous layer of height H and refractive index of $n_1 = 2.95$ (blue) and $n_2 = 2.11$ (black) on top. These indices correspond to the values of effective refractive indices calculated for TE and TM transmissions propagating through the metalMHCG (see Section II in main text). Although the periodicity of transmission with respect to H is equal in both cases indicated by the same colors (metalMHCG and homogenous layer), the amplitudes of transmissions are significantly different, which is attributed to the presence of the metal in the metalMHCG case.

light was then directed to a HgCdTe (MCT) liquid-nitrogen cooled detector and transferred as an electrical response into an analog-to-digital converter. The signal was later modified using a 3-Term Blackman-Harris apodization function or an adequate zero-filling factor and converted into a spectrum using Fast Fourier Transform. To perform polarization-resolved measurements, a KRS-5 wire-grid polarizer was inserted into the beam path before the light reached the sample, as shown in S4b. Using this experimental procedure, we were able to obtain spectra in the 1.3–15 µm spectral range with a 4 cm^{-1} resolution.

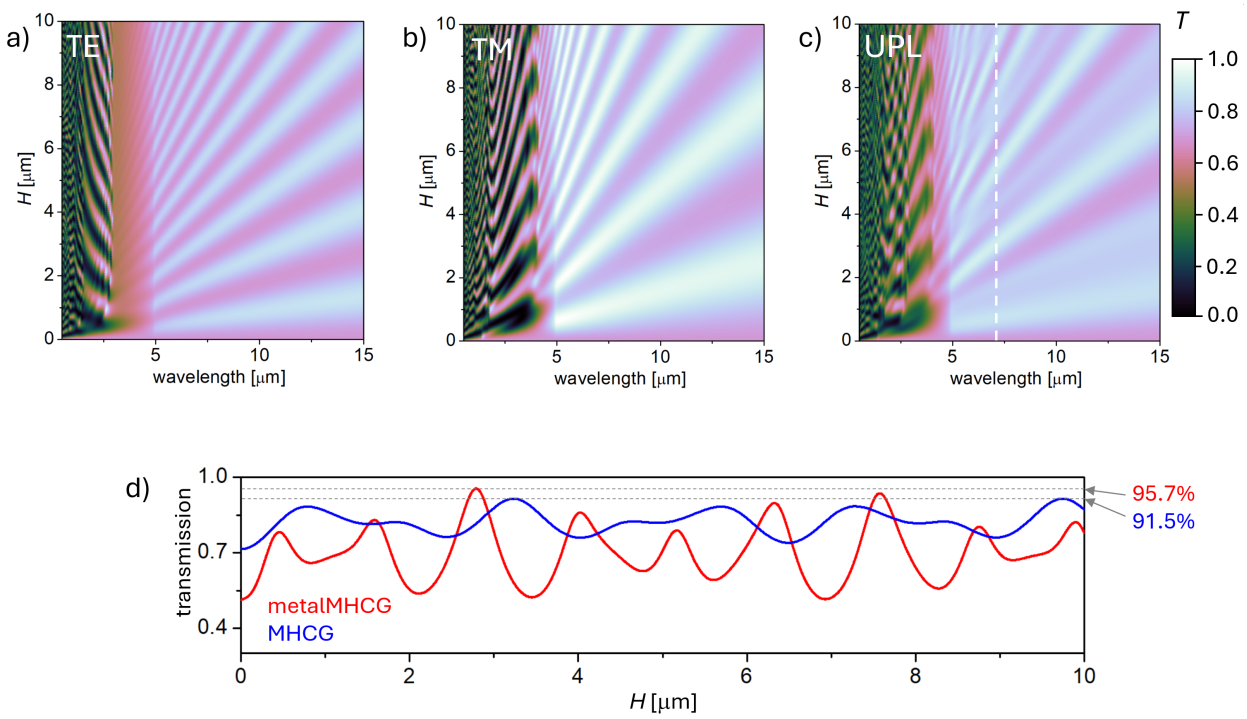

Figure S3. Calculated transmission (T) maps of the MHCG (without gold) under normal incidence of a) TE, b) TM polarized light, c) unpolarized light in the domain of the wavelength, and height of the semiconductor stripes (H), the dashed white line indicates the wavelength used in d); d) unpolarized transmission as a function of the stripe height for the MHCG (blue) and metalMHCG (red). The paramaters of the MHCG and the metalMHCG are $L = 1.4\,\mu\text{m}$, $F = 0.56$ and $L = 1.4\,\mu\text{m}$, $F = 0.74$, respectively.

S2. COMPARISON OF EXPERIMENTAL AND NUMERICAL SPECTRA FOR THE ACTUAL METALMHCG CROSS-SECTION

To compare the experimental spectrum with the numerically computed spectrum (Fig. S5a), we implemented the metalMHCG cross-section derived from the SEM image (Fig. S5b), as seen in Fig. S5c, in PLaSK software [5], which was used for all calculations in this study. In Fig. S5a, the experimentally measured spectrum (black line) is shown alongside three numerically computed spectra. The green dashed line corresponds to the spectrum calculated using the optimal parameters for a rectangular metalMHCG cross-section (rectangular), with the parameters defined in Table I (first row). The blue dashed line represents the spectrum computed based on the cross-section and geometric parameters (SEM), extracted

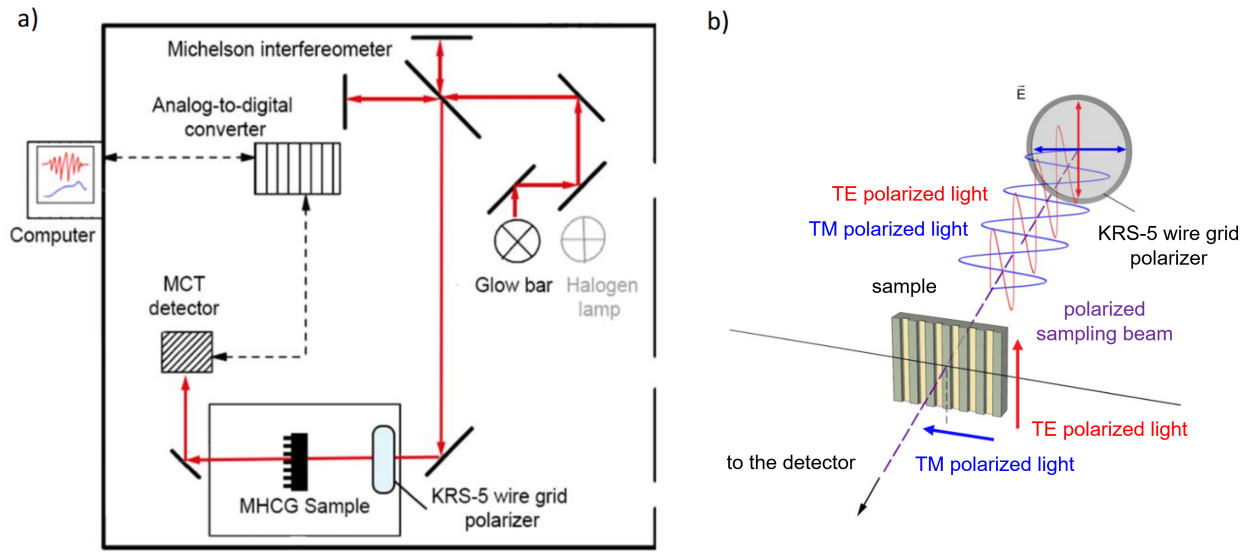

Figure S4. a) Schematic view of the beam path in a transmittance experiment with FTIR setup; b) close-up of polarizer mounting showing the direction of stripes in the sample

from the SEM image (see Table I, second row). The red solid curve represents the spectrum obtained by optimization using the SEM-derived cross-section and metalMHCG parameters (L, F, H) to minimize the sum of squared differences between the experimental and computed spectra (first and third rows in Table I).

All curves are closely aligned, accurately identifying both the positions and values of the transmission maxima and minima. The red curve, resulting from the optimization procedure, exhibits the closest match to the experimental data. By comparing the metalMHCG parameters in Table I, it can be observed that the height (H) extracted from the SEM image differs noticeably from the value obtained through the optimization procedure. The SEM-based height measurement may be inaccurate due to charging effects at the surface of undoped GaAs. As a result, the height (2.847 µm) derived from SEM image may be overestimated, as suggested by the result of optimization procedure, where the height H is determined to be 2.7 µm.

S3. INFRARED PHOTOGRAPHY

To compare the transmission through the GaAs substrate and the GaAs substrate with metalMHCG, a thermal imaging experiment was carried out. A QR code was manufactured

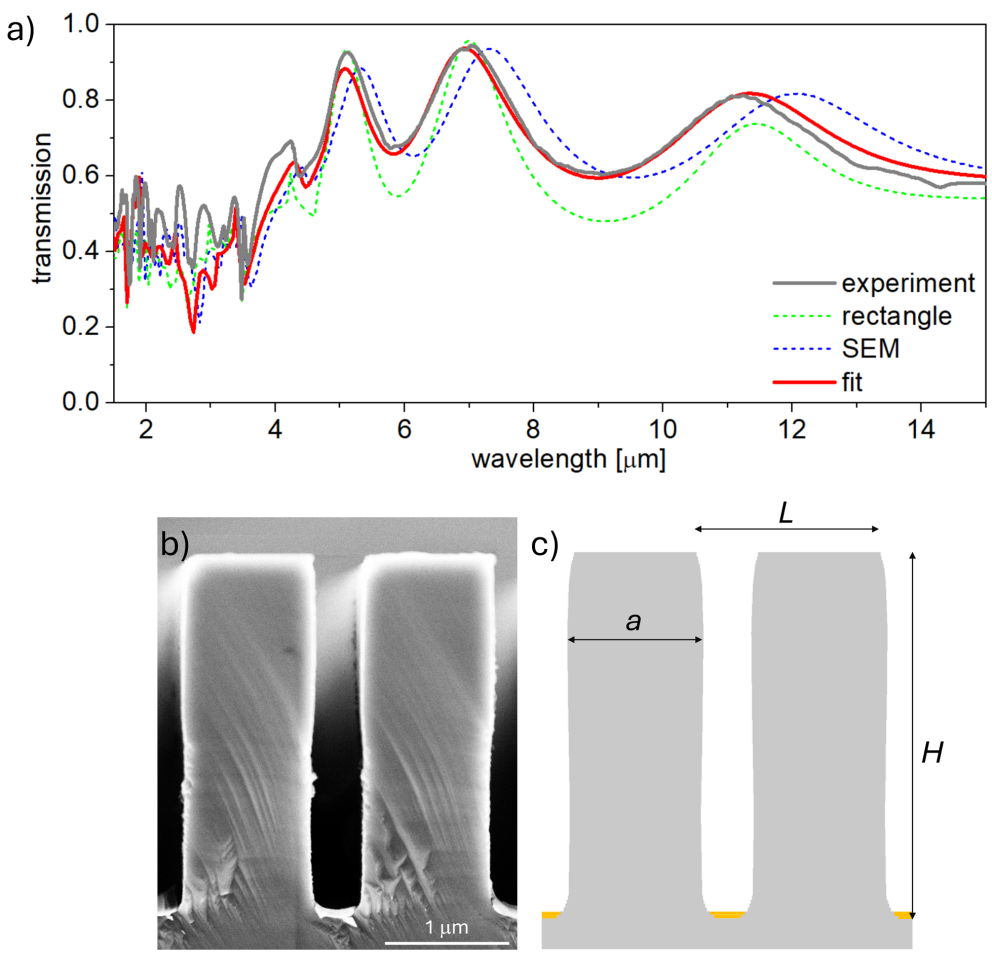

Figure S5. a) Experimental (black line) and calculated (other lines) spectra of the metalMHCG with geometrical parameters defined in Table I; b) cross-section scanning electron microscope (SEM) image of metalMHCG; c) image of the metalMHCG implemented in the numerical algorithm.

Table I. Geometrical parameters of the metalMHCG for various cross-section shapes.

	L [μm]	$F = a/L$	H [μm]	Cross-section
rectangle	1.431	0.734	2.787	Rectangle
SEM	1.47	0.759	2.847	SEM image
fit	1.465	0.745	2.699	SEM image

on a FR4 PCB laminate, providing a strong emissivity contrast to the copper-made code. The dimensions of the code were chosen taking into account minimum focusing distance of the thermographic camera lens and the the limits its instantaneous field of view (IFOV). The QR code was placed on a heatbed and imaged using a FLIR X6901SC InSb cooled

thermographic camera operating in the 3–5 µm band. The camera was equipped with an extension ring and a 4.8–5.0 µm band-pass optical filter. The spectral characteristics of the optical filter in the proximity of fourth transmission band are illustrated in Fig. S6a. The 1/4 inch ring was used for magnification, short enough to avoid image vignetting. As the filter considerably reduced the energy reaching the camera detector matrix, the code was heated to the temperature of 80°C using the heatbed and the camera integration time was adjusted. The GaAs substrate and the GaAs substrate with metalMHCG were placed in a dedicated 3D printed sample holder with a narrow slot, allowing for easy movement of both samples above the QR code and subsequent acquisition of the code thermograms through both samples, column by column. A series of 9 thermograms was taken and the fragments of the thermograms obtained through the slot were merged together, obtaining a final thermogram of the complete QR code. A picture of the code is shown in Fig. S6a and an image of the sample holder with both samples and the code visible beneath is shown in Fig. S6b. The complete test setup is shown in Fig. S7.

[1] Thermofisher.com, accessed: 2023-07-21.

[2] P. R. Griffiths and D. H. J. A., *Fourier transform infrared spectrometry* (Wiley, 2007).

[3] M. Motyka and J. Misiewicz, Applied Physics Express **3**, 10.1143/APEX.3.112401 (2010).

[4] M. Motyka, G. Sek, F. Janiak, J. Misiewicz, K. Klos, and J. Piotrowski, Measurement Science and Technology **22**, 125601 (2011).

[5] Plask.com, accessed: 2026-06-08.

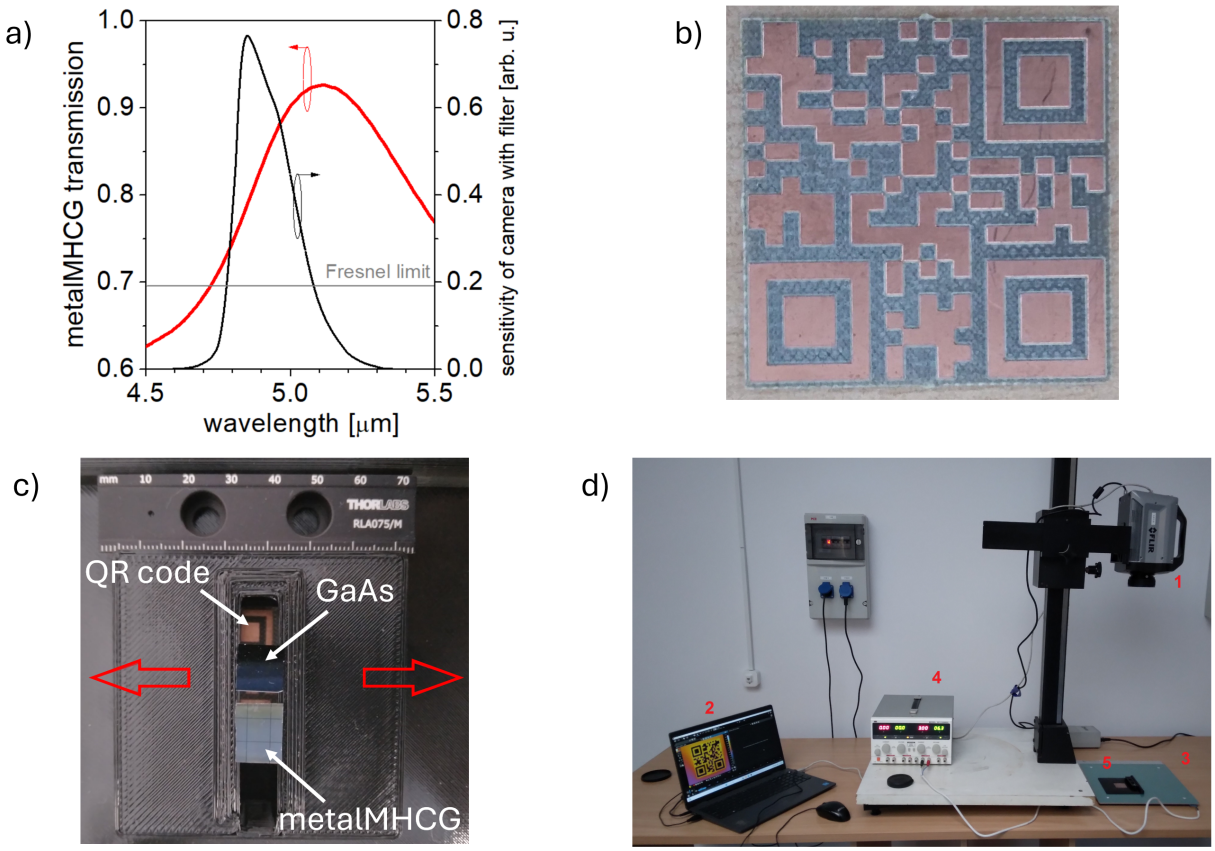

Figure S6. a) Transmission spectrum in the proximity of fourth transmission band (red line, left axis) and spectral sensitivity of the camera with filter (black line, right axis), b) visible light picture of the 21×21 QR code fabricated on FR4 PCB laminate used for thermographic imaging; c) the holder with GaAs sample (top) and metalMHCG sample (bottom) and the code visible underneath through the slot, d) the test setup used for thermographic visualisation: 1. thermographic camera; 2. camera control computer; 3. heatbed; 4. heatbed DC power supply; 5. QR code.

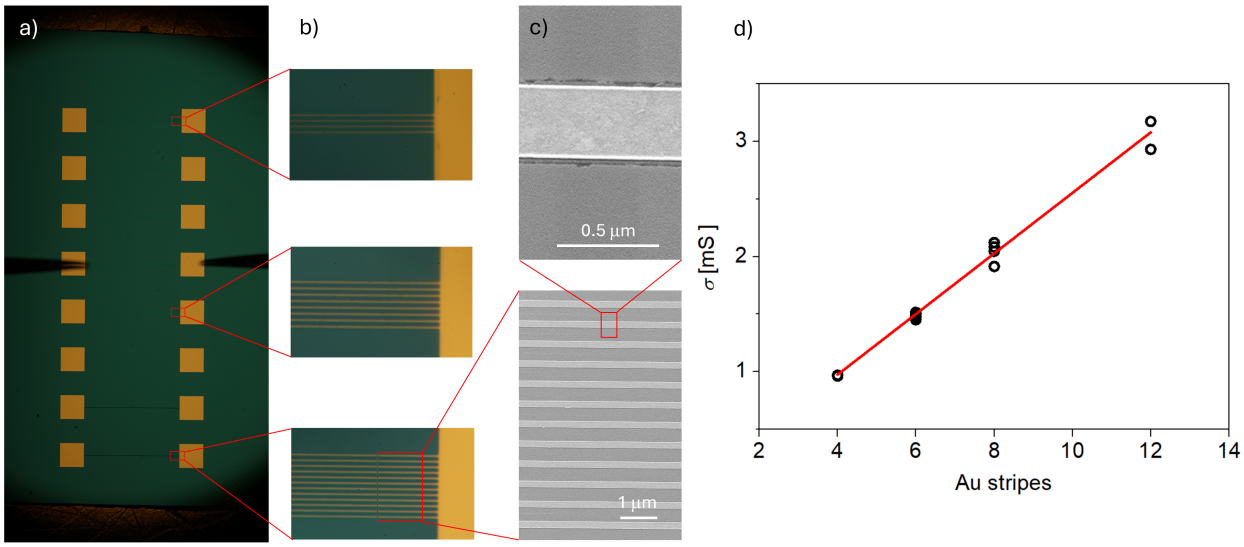

Figure S7. Visible microscope images of (a) gold pads and (b) 50 nm-thick gold wires, along with their (c) corresponding SEM images, intended for electrical conductivity characterization; d) conductance measured for different number of gold stripes.